Experimental and Numerical Parameter Study of a Helmholtz Resonator with a Flexible Wall

Fleming Kohlenberg*
Technische Universität Berlin, 10623 Berlin, Germany,
now: *German Aerospace Center (DLR), 10625 Berlin, Germany*

Karsten Knobloch†
German Aerospace Center (DLR), 10625 Berlin, Germany

Modern aircraft engines have a large bypass ratio for fuel efficiency but consequently emit more low-frequency noise, which cannot be damped efficiently with conventional perforate-over-honeycomb liners. In this paper, a Helmholtz resonator is combined with a flexible plate subdividing the cavity to allow for resonances below the conventional Helmholtz resonance. This concept is investigated experimentally and numerically in a normal incidence tube to determine the impacts of the face sheet, the cavity dimensions and the flexible wall materials. Additional microphones are implemented inside the resonator to successfully separate Helmholtz and plate resonances. A numerical model was developed, validated with experimental results and used to resolve the impact of key parameters. We found that the face sheet and main cavity mainly alter the Helmholtz resonance and that the plate related resonances show great sensitivity towards the back cavity size and the material and size parameters. These results give valuable insight into the working principles of the concept and show the great adaptivity for future optimization and application.

Nomenclature

f_{HR}	=	Helmholtz resonance frequency
c_0	=	speed of sound in air
n	=	number of holes in face sheet
d_{fs}	=	face sheet orifice diameter
A_{cav}	=	cavity cross section
l_{cav_1}	=	main cavity depth
h_{fs}	=	face sheet thickness
δ_{m}	=	additional mass
σ	=	face sheet open area
$f_{i,j}$	=	plate eigenfrequency
λ	=	eigenfrequency parameter
l_{p}	=	flexible plate length
E	=	Young's modulus
h_{p}	=	flexible plate thickness
ρ_{p}	=	flexible plate density
ν_{p}	=	flexible plate Poisson's ratio
i	=	imaginary number
k	=	wave number
ω	=	angular frequency
x	=	distance to reference plane
$\hat{p}^+$	=	sound pressure of the incident plane wave
$\hat{p}^-$	=	sound pressure of the reflected plane wave

*PhD candidate, Dept. of Engine Acoustics (DLR-AT-TRA), AIAA Student Member, fleming.kohlenberg@dlr.de
†Scientist, Dept. of Engine Acoustics (DLR-AT-TRA)

This is the author's version of the work that was accepted for publication in the proceedings of the
30th AIAA/CEAS Aeroacoustics Conference held in Rome, Italy in June 2024.
The final version was published in the proceedings of the conference as paper no. 2024-3077: https://arc.aiaa.org/doi/10.2514/6.2024-3077

p'	=	measured sound pressure
r	=	reflection coefficient
α	=	normal incidence absorption
Z	=	specific impedance
ζ	=	normalized specific impedance
θ	=	normalized specific resistance
χ	=	normalized specific reactance
ρ_0	=	density of air
η	=	material loss factor
l_{cav_2}	=	back cavity depth
ζ_{fs}	=	face sheet normalized specific impedance
δ_{resist}	=	resistive end correction
δ_{react}	=	reactance end correction
ψ	=	hole interaction function
F	=	function to account for viscous wall effects
k_{s}	=	Stokes wave number
ν	=	kinematic viscosity
α_{tot}	=	overall absorption
ζ_{tot}	=	overall normalized impedance
α_{cav}	=	back cavity and flexible wall absorption
ζ_{cav}	=	back cavity and flexible wall normalized impedance

I. Introduction

To reduce the environmental impact of civil aviation, the European Commission has set ambitious goals for 2050: "Increase the fleet fuel efficiency (30-50 % relative to 2018 levels) and reduce the perceived perceived noise emission of flying aircraft (65 % per operation relative to the 2000 baseline)"[1]. To meet these goals, aero-engines will need to increase their bypass ratio and consequently their fan size, while maintaining low weight and drag. A larger fan with a reduced rotation frequency is expected to be quieter but emits fan noise with lower frequency tonal noise, which is a challenge for conventional liners. These conventional liners work similar to a Helmholtz resonator. Their maximum absorption frequency at resonance can be tuned towards lower frequencies by enlarging their back cavity. However, these cavity depths are limited due to installation space constraints in the nacelle, as a large cowl would lead to more drag and consequently more fuel consumption. Inevitably, we need new liner concepts to damp low-frequency noise.

One approach to broaden the absorption spectrum of Helmholtz resonators is to combine them with mechanical elements, such as membranes [2–7] or flexible plates [8–13], which have the benefit of being tunable independent of the Helmholtz resonance. Moreover, this way low-frequency noise can be damped without increasing the overall resonator volume.

Knobloch et al. [14] used flexible walls in a liner segment to couple cavities proving that the concept of integrating flexible walls is beneficial for low-frequency broadband damping. Kohlenberg et al. [12] developed an analytical model to predict the impedance of a Helmholtz resonator with a small circular plate subdividing the cavity. They found good agreement with their experimental data, but the model was limited to cases where only the first radial mode is dominant. In a later work [15], they showed that in a system with larger circular plates, multiple radial modes contribute to the overall damping. With the help of a vibrometer setup, they could separate Helmholtz resonances and plate associated resonances and found stronger plate vibration when Helmholtz resonance and plate resonances were close together. Using the same resonator system, Genßler et al. [16] experimentally investigated the position and number of flexible plates, as well as its materials, shapes and size. They found the plate material and especially its flexural rigidity to be the most sensitive parameter and concluded that a low flexural rigidity is beneficial.

In this paper these works are extended experimentally and numerically with a special focus on the working principles of the flexible plate. Instead of a global optimization scheme, the idea is to investigate the influences of key parameters to gain more insights into the system's response. The experimental part serves two purposes. The normal incidence tube in combination with additional instrumentation inside the cavities allows us to separate the effect of the flexible plate from the whole system. Additionally, it is a validation basis for the numerical simulations. These numerical simulations allow us to alter single parameters such as the material damping alone which would be hardly feasible by experimental design. Furthermore, they are able to resolve the acoustic field inside the resonator and the full motion of the flexible

plate.

The resonator concept has the advantage of a very extensive parameter space which all alter the acoustic damping behavior, as it combines structural resonances with fluid resonances. The goal of this paper is therefore to gain more insights into how these parameters affect the overall damping. With this knowledge, the parameter space can be reasonably constrained for future optimization and the results better interpreted.

Two analytical key predictor sets are important to determine the most important parameters: The Helmholtz resonance frequency, and a list of the in-vacuo eigenfrequencies of the flexible plate. The Helmholtz resonance frequency

$$f_{\mathrm{HR}} = \frac{c_0}{2\pi}\sqrt{\frac{\sigma}{l_{\mathrm{cav}_1}(h_{\mathrm{fs}} + \delta_{\mathrm{m}})}}, \tag{1}$$

predicts the frequency with the maximum sound velocity in the face sheet holes and consequently the maximum damping. In Eq. (1) c_0 denotes the speed of sound, $\sigma = n\pi/4\, d_{\mathrm{fs}}^2/A_{\mathrm{cav}}$ the open area ratio, n the number of face sheet holes, d_{fs} the face sheet hole diameter, A_{cav} the cavity cross section, h_{fs} the face sheet thickness and l_{cav_1} the (main) cavity depth. δ_{m} is a mass end correction term, which can be approximated after Ingard [17] by $\delta_{\mathrm{m}} = 8/(3\pi)(1 - 1.25\,\sigma)d_{\mathrm{fs}}$. However, as Eq. (1) is derived assuming rigid walls and no flow separation, the effect of the flexible plate and possible nonlinear effects are disregarded.

The other key predictors are the in vacuo eigenfrequencies of the flexible plate, where the flexible plate can be excited the easiest and the maximum plate velocity is obtained. They can be calculated analytically, e.g. for a rectangular clamped plate with side length l_{p}:

$$f_{ij} = \frac{2\lambda_{ij}}{\pi l_{\mathrm{p}}^2}\sqrt{\frac{E h_{\mathrm{p}}^2}{12\rho_{\mathrm{p}}(1-\nu_{\mathrm{p}}^2)}}, \tag{2}$$

with λ_{ij} denoting the horizontal and vertical eigenfrequency parameter, E Young's modulus, h_{p} the flexible plate thickness, ρ_{p} the flexible plate density and ν_{p} Poisson's ratio [18]. Expected crucial plate parameters are therefore: E, h_{p} and l_{p}.

Precisely, we want to investigate the following questions in this paper:

- Which parameter affects the Helmholtz resonance, which parameter affects flexible wall resonances and which affects both? For example, does a change in flexible wall rigidity affect the Helmholtz resonance? How do these parameters project onto the overall damping?
- How do geometrical changes e.g. of the face sheet or cavities project onto the flexible plate's response and
- Which plate properties are beneficial? How much does the structural damping contribute to the overall damping?

This paper is structured in the following way: Details about the measurement setup can be found in Section II, while the numerical setup is presented in Section III. Section IV includes the presentation and discussion of the experimental and numerical results. The paper is completed with a conclusion drawn in Section V.

II. Experimental setup

We investigate the resonator system experimentally in the normal incidence tube (D-NIT) of the Department of Engine Acoustics of the German Aerospace Center (DLR-AT-TRA) in Berlin. The normal incidence impedance tube has a square cross section of 35 mm × 35 mm and therefore a cut-on frequency of the first higher mode of 4900 Hz. In the basic configuration, the sound source is one upstream loudspeaker (BMS-4599-ND) attached to the duct end opposite to the probe. The extended configuration consists of four loudspeakers of the same model attached to the four side walls. We use a multi-microphone method with three microphones (G.R.A.S 46BD-FV ¼") flush mounted in the measurement section to decompose the sound field in incoming and reflecting acoustic waves. The resulting equation system

$$\underbrace{\begin{bmatrix} \mathrm{e}^{-\mathrm{i}kx_1} & \mathrm{e}^{\mathrm{i}kx_1} \\ \mathrm{e}^{-\mathrm{i}kx_2} & \mathrm{e}^{\mathrm{i}kx_2} \\ \mathrm{e}^{-\mathrm{i}kx_3} & \mathrm{e}^{\mathrm{i}kx_3} \end{bmatrix}}_{\boldsymbol{A}} \underbrace{\begin{bmatrix} \hat{p}^+ \\ \hat{p}^- \end{bmatrix}}_{\boldsymbol{x}} = \underbrace{\begin{bmatrix} p'(x_1) \\ p'(x_2) \\ p'(x_3) \end{bmatrix}}_{\boldsymbol{b}}, \tag{3}$$

is fitted in a least-square sense by calculating $x = \boldsymbol{A}^+ b$, with $\boldsymbol{A}^+$ denoting the pseudo inverse of $\boldsymbol{A}$. In Eq. (3), i denotes the imaginary unit, $k = \omega/c$ the (plane) wavenumber as the quotient of angular frequency ω and speed of sound c, $p^{\pm}$

the incoming and reflected sound wave respectively and $p'(x_n)$ the measured sound pressure at the distance x_n from the reference plane. The microphones are attached at a distance of $x_1 = 110\,\text{mm}$, $x_2 = 145\,\text{mm}$ and $x_3 = 220\,\text{mm}$ to the probe, where the near field of the loudspeakers and probe have sufficiently vanished. Using three microphones instead of two, allows us to avoid singularities in the pseudo-inverse and to determine a measured error between measured and fitted sound pressure field. One additional microphone is attached as close as possible to the reference plane to measure the sound pressure level at the probe. The viscothermal losses inside the duct walls are taken into account as proposed by Dokumaci [19]. We choose the direct incidence setup due to the straightforward determination of the acoustic impedance. Based on the decomposed waves, the complex reflection factor of the sample $r = {}^{p^-}/_{p^+}$ can be calculated. This reflection factor is then used to calculate the absorption $\alpha = 1 - |r|^2$ and the complex normalized impedance

$$\zeta = {}^{Z}/_{\rho_0 c_0} = \theta + \mathrm{i}\chi = \frac{1+r}{1-r}, \tag{4}$$

where θ is the specific normalized resistance and χ the specific normalized reactance.

We investigate a Helmholtz resonator with a flexible wall which consists of a face sheet, a main cavity, a flexible plate and a second cavity, similar to the resonator system previously studied in [12, 15, 16]. The modular setup allows the change of the face sheet, the flexible plate, and the back cavity depth. Furthermore, we attached two microphones inside the main cavity and one in the back cavity to resolve the sound fields inside the resonator system. A sketch and a photograph of the measurement setup is depicted in Fig. 1.

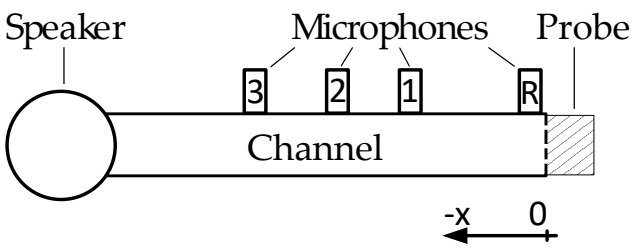

(a) Sketch of the D-NIT with the resonator system placed at the upstream end

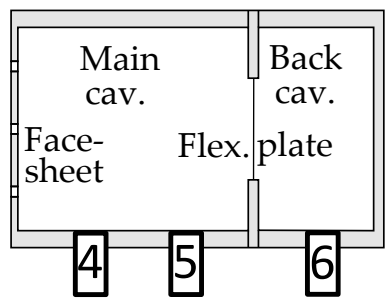

(b) Sketch of the probe / resonator system with microphones

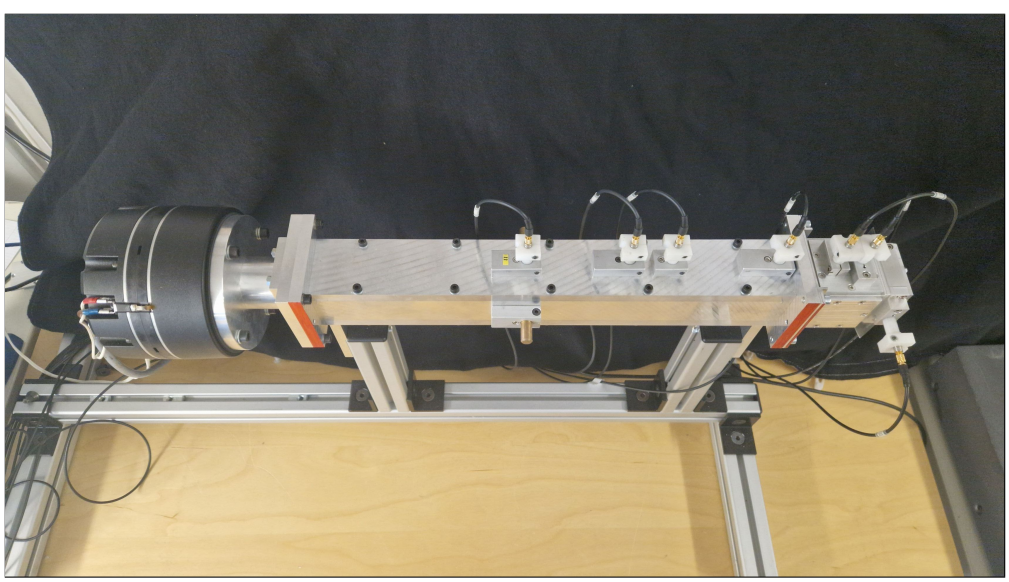

(c) Photograph of the measurement setup

Figure 1 Experimental setup to investigate Helmholtz resonators with flexible walls at the D-NIT

In the linear region, the sound waves are excited with a swept sine and an incoming plane wave amplitude of below

90 dB. In this region, the resonator system's acoustic properties are independent of the incident amplitude.

We use the two additional microphones 4 and 5 inside the main cavity to decompose the sound field in back and forth travelling sound waves analogous to the impedance tube to determine the impedance ζ_{cav} and absorption α_{cav} of just the flexible wall with the back cavity. The additional microphones are positioned very close to both the face sheet and the flexible plate due to the small size of the resonator. Even though less robust results are expected due to the corresponding near-fields, the method allows us to separate plate and face sheet related phenomena without extensive laser vibrometer measurements. Microphone 6 is used to quantify the pressure drop between main and back cavity which is thought to be the main driving force of the plate oscillation.

The resonator system core has the same cross section as the normal incidence tube of 35 mm × 35 mm. The regular cavity walls are made out of aluminum with a thickness of 10 mm and therefore can be considered acoustically rigid. The main cavity depth is $l_{\text{cav}_1} = 60$ mm and the back cavity depth is $l_{\text{cav}_2} = 15$ mm. The flexible wall between both cavities is interchangeable in size, shape and material and clamped between two plate holders with a variable cut-out. For this study a rectangular cut out of 15 mm × 26 mm was chosen. We tested three different face sheets and three different materials in the normal incidence tube. The face sheet properties are reported in Table 1 and are appended by the corresponding Helmholtz resonance frequency f_{HR}, calculated with Eq. (1) by assuming rigid walls and a single cavity depth of $l_{\text{cav}_1} = 60$ mm.

The flexible wall material data is presented in Table 2. Since the flexible wall is not prestressed, the restoring forces result from its stiffness. Therefore, we model the flexible wall as a plate. The Young's Modulus E and loss factor η for the polymers Thermpolyurethan (TPU) and Ethylenbutylacrylat (EBA) were determined by a dynamic mechanical analysis and are both temperature and frequency dependent. The values given in Table 2 are at ambient conditions for low frequencies. For the third material, Aluminum, we assumed standard textbook values. A photograph of the samples

Table 1 Face sheet properties and corresponding Helmholtz resonance frequency

Face sheet	h_{fs} in mm	d_{fs} in mm	σ_{fs} in %	f_{HR} in Hz
I	2	1.5	2.6	631
II	2	1	1.2	449
III	1	1	4.1	1062

Table 2 Flexible plate properties

Material	E in MPa	η	h_{p} in mm	ρ_{p} in kg/m^3	ν
TPU	16	0.1	0.3	1080	0.49
EBA5	10.5	0.09	0.55	940	0.49
Alu	70000	0.005	0.05	2700	0.33

is depicted in Fig. 2

The first five eigenfrequencies for the different material probes calculated with Eq. (2) are listed in Table 3. All materials have eigenfrequencies within the investigated frequency range of the normal incidence tube. Note, that the lowest three eigenmodes all correspond to the longer side of the material probe (26 mm).

Table 3 Lowest five plate eigenfrequencies for the clamped plate samples

Material	$f_{0,0}$ in Hz	$f_{1,0}$ in Hz	$f_{2,0}$ in Hz	$f_{0,1}$ in Hz	$f_{3,0}$ in Hz
TPU	219	308	462	556	680
EBA5	372	523	785	944	1154
Alu	1412	1985	2982	3585	4383

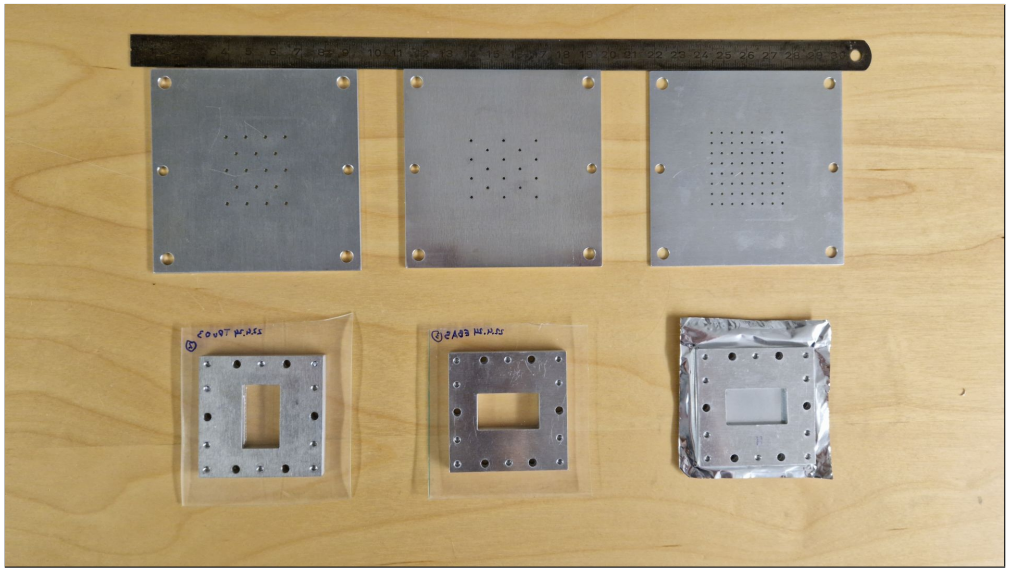

Figure 2 Photograph of the face sheet samples and material probes

III. Numerical setup

The normal incidence tube and resonator system are modeled with the commercial finite element software COMSOL Multiphysics® 6.1. The numerical model allows us to investigate the impedance, absorption and plate displacement of the resonator system. This setup enables us to examine key parameters such as the pressure field inside the resonator and the plate vibration which are hard to determine experimentally. Furthermore, parameter variations not possible with purely experimental methods such as a variation of the material dependent loss factor in the plate to investigate its impact may be implemented.

There are two approaches to include the face sheet in the simulation environment: simulate the fluid domain and boundary layers in the face sheet holes or model it as an impedance boundary condition. Resolving the fluid domain in the holes requires much more computational effort, especially when dealing with nonlinear effects such as flow separation. The focus of this work are the interdependencies between the flexible plate and the rest of the resonator system for which we found the impedance boundary condition to be sufficiently accurate. The face sheet is, therefore, modeled by an impedance boundary condition

$$\zeta_{\mathrm{fs}} = -\mathrm{Re}\left(\frac{\mathrm{i}\omega}{c_0\sigma}\frac{2\delta_{\mathrm{resist}}}{F}\psi(\sigma)\right) - \mathrm{Im}\left(\frac{\mathrm{i}\omega}{c_0\sigma}\frac{2\delta_{\mathrm{react}}}{F}\psi(\sigma)\right), \tag{5}$$

$$F = \frac{J_2(k_s d_{\mathrm{neck}}/2)}{J_0(k_s d_{\mathrm{neck}}/2)}, \quad k_{\mathrm{s}} = \sqrt{-\frac{\mathrm{i}\omega}{\nu}}, \tag{6}$$

with δ_{resist} and δ_{react} denoting the resistive and reactive end correction respectively [20]. Eq. (6) is based on [21]. F is a function to account for viscous effects at the hole walls and depends on the Bessel functions of the first kind of zeroth J_0 and second order J_2 and the Stokes wave number k_{s}. ν is the kinematic viscosity. $\psi(\sigma)$ is a function to account for hole interactions [22].

The flexible plate is modelled as a 2-D shell structure. Otherwise, resolving the 3-D structure inside the thin (< 1 mm) plate would require an unnecessary fine mesh, which we disregarded. A mesh refinement study of the model, not shown here, revealed that ten elements per relevant length scale (smallest side length) are sufficient to resolve the plate behavior, while six quadratic elements per wavelength in the air domain are sufficient to resolve the acoustic field. The mesh and an exemplary plot of the pressure field and the plate deflection shape can be found in Fig. 3.

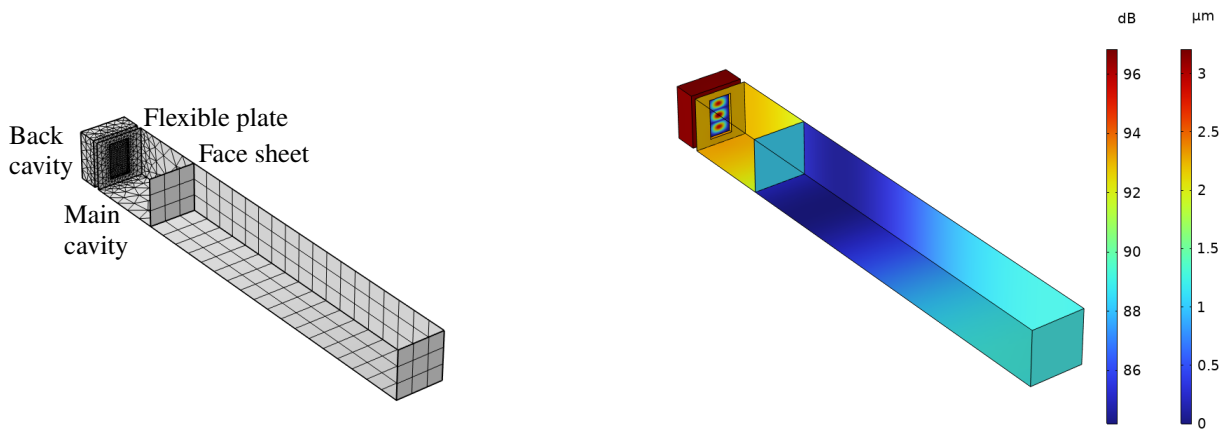

(a) Mesh overview of the numerical setup

(b) Exemplary sound pressure level field and plate deflection at 455 Hz

Figure 3 Numerical setup and exemplary sound field and plate deflection

IV. Results and Discussion

In this section the experimental and numerical results of the measurements with respect to different parameters are presented and discussed. The section starts with the experimental results.

A. Experimental results

Figure 4 displays the experimental results of the baseline configuration of the resonator system with face sheet I and a flexible wall made out of TPU (material 1). The blue line is the measured overall absorption coefficient α_{tot} as

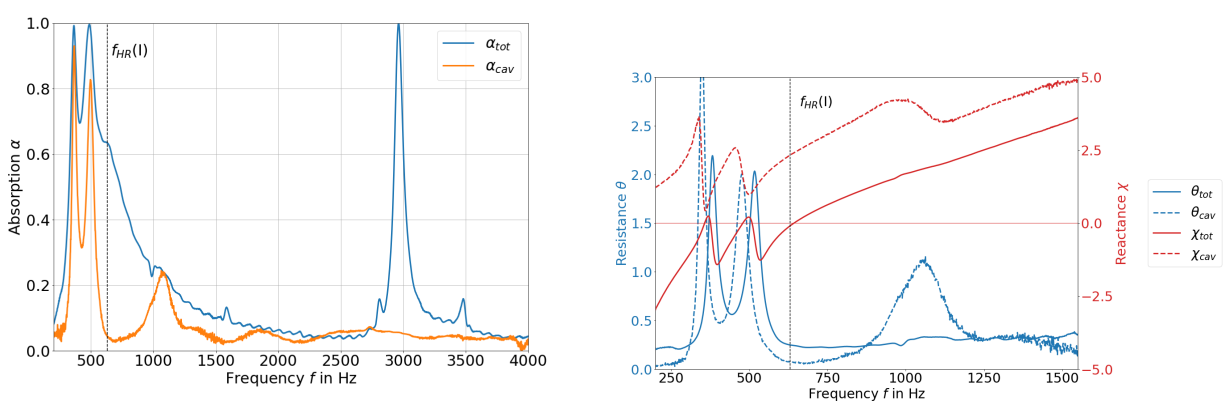

(a) Overall (blue) absorption and absorption of only the flexible plate and back cavity (orange) of the resonator with face sheet I and material 1 (TPU)

(b) Overall (solid) impedance and isolated impedance of the flexible plate and back cavity (dashed) of the resonator with face sheet I and material 1

Figure 4 Comparison between overall and plate related behavior

determined by the plane wave decomposition using microphones 1–3. The orange line is the measured absorption coefficient α_{cav} which includes the isolated effect of the back cavity and the plate holder with the flexible plate. The latter coefficient is determined with microphones 5 and 6, which are installed inside the main cavity. The overall absorption spectrum (blue) shows high absorption around 360 Hz, 470 Hz and to a minor degree around 630 Hz and 1100 Hz. In comparison, the absorption spectrum of the plate and back cavity (orange) displays only absorption peaks around 360 Hz, 470 Hz and 1100 Hz. Therefore, these peaks can be attributed to plate related resonances while the other peaks are

related to the Helmholtz resonance, which only appear when the main cavity and face sheet are present. At the Helmholtz resonance, the (main) cavity is compressed uniformly which fulfills the resonance condition of a pressure maximum at the back and a particle velocity maximum at the face sheet. This resonance condition is also met with a pressure node in the middle of the cavity (higher cavity mode) around 3000 Hz, which is visible as a sharp absorption peak in the overall absorption. Note, that this frequency is not a harmonic of the Helmholtz resonance frequency $f_{\mathrm{HR}} = 630\,\mathrm{Hz}$ due to the presence of the face sheet.* The corresponding normalized impedance ($\zeta = \theta + \mathrm{i}\chi$)blue: resistance, red: reactance), focused on frequencies below 1500 Hz is displayed in Fig. 4b. The overall impedance is plotted as a solid line where the zero-crossings of the reactance with a positive slope correspond to a resonance with a high absorption. A zero-crossing of the reactance with a negative slope corresponds to an anti-resonance with a sharp increase of the resistance which leads to a reduced absorption. Note that in the normal incidence case, maximum absorption is achieved at $\zeta = 1 + \mathrm{i}\,0$. The reactance of the back cavity and the plate holder with a flexible plate (dashed) appears to have a similar pattern, but shifted towards higher values. The reactance of the back cavity can be approximated by $\zeta_{\mathrm{bc}} = \frac{1}{\mathrm{i}k\tan\left(kl_{\mathrm{cav}_2}\right)}$, which has a positive slope in the investigated frequency range and the distinctive shape can be therefore attributed to the plate impedance which is dominated by resonances. These trends agree with previous results from the authors for a Helmholtz resonator system with a circular plate. [23]

The results for the system with the same plate material but with different face sheets are presented in Fig. 5. Face

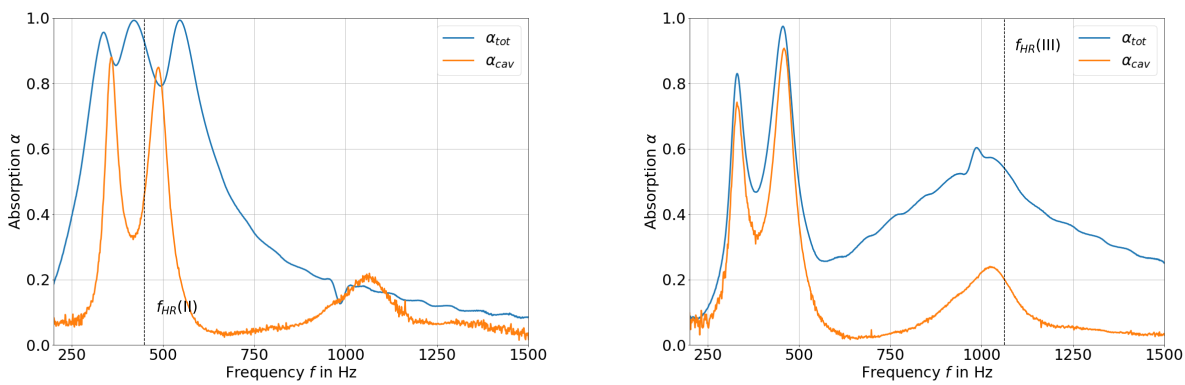

(a) Absorption Face sheet II with Material 1 (TPU) **(b) Absorption Face sheet III with Material 1 (TPU)**

Figure 5 Measured absorption and impedance of the baseline configuration (face sheet I and material I)

sheet II has a lower porosity and according to Eq. (1) a lower Helmholtz resonance. The effect of the lower porosity can be observed in Fig. 5a, as the peak associated with the Helmholtz resonance is in this case around 550 Hz. The Helmholtz resonance and the two low frequency absorption peaks of the whole resonator system (blue) all have changed to lower frequencies. However, the absorption spectrum of only the back cavity and flexible plate (orange) reveals that the response of the flexible plate has not changed with a different face sheet. Note, that the orange absorption peaks are at higher frequencies than the blue overall absorption peaks. This means that in the linear case a face sheet change alters the overall response and the overall additional absorption peaks differ from the plate resonances but the underlying plate behavior remains unchanged. The Helmholtz resonance on the other hand has shifted towards higher frequencies from $f_{\mathrm{HF(I)}} = 450\,\mathrm{Hz}$ to 550 Hz due to the flexible wall. A similar behavior can be found in Fig. 5b with face sheet III and a higher Helmholtz resonance. In this case the Helmholtz resonance is far off the first plate resonances and the overall absorption at these peaks are very similar to the plate and back cavity resonances alone.

B. Comparison between experimental and numerical results

A comparison between measurements and simulations of the baseline configuration are presented in Fig. 6. A very good agreement between the experimentally (blue) and numerically (orange) determined absorption spectra can be found in Fig. 6a for both the plate related resonances, as well as the Helmholtz resonance. Thus, the numerical model is able to capture the relevant phenomena very well. A closer look at the corresponding impedance in Fig. 6b, focused on

*This distinguishes the Helmholtz resonator from a simple quarter-wave resonator, which has m harmonic resonances $\frac{c_0}{l_{\mathrm{cav}_1}}\left(\frac{1}{4} + \frac{m}{2}\right)$.

the low frequency region, shows a very good agreement too. However, differences near the first resonance at 360 Hz in both the reactance (red) and resistance (blue) are visible which might be due to experimental uncertainties such as material parameters or uncontrolled pretension of the flexible wall. The absorption spectra for the resonators with

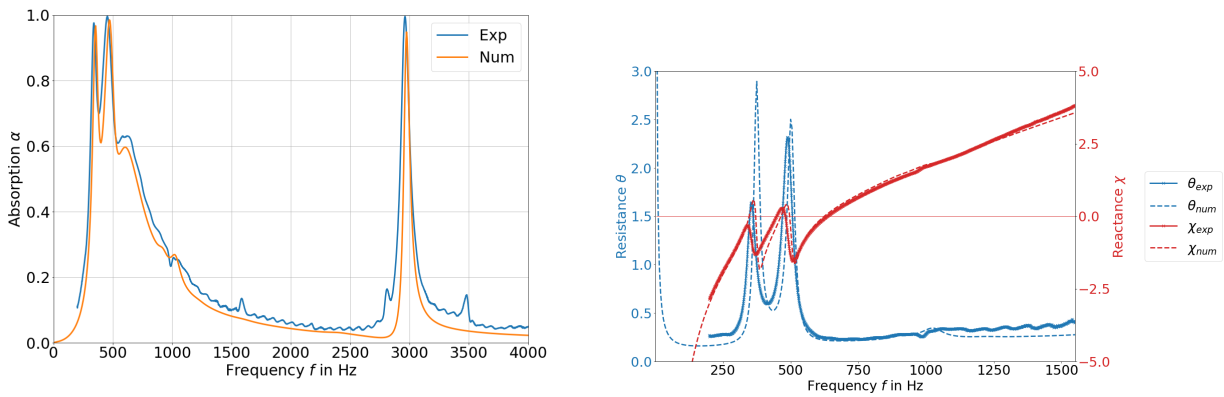

(a) Absorption **(b) Normalized impedance**

Figure 6 Comparison between numerical and experimental results of face sheet I with material 1

different face sheets determined experimentally and numerically are displayed in Fig. 7. The effect of a changing face sheet is captured very well in the numerical setup too, as the lines agree very well.

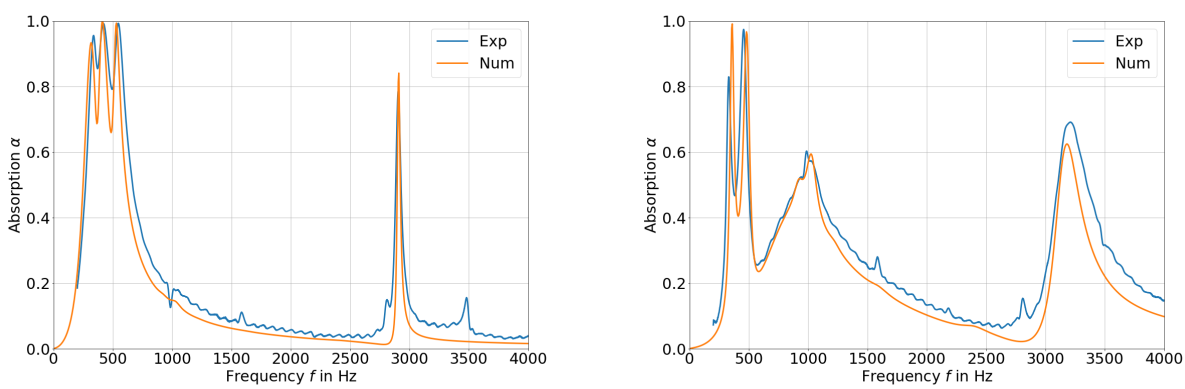

(a) Absorption face sheet II with material 1 (TPU) **(b) Absorption face sheet III with material 1 (TPU)**

Figure 7 Comparison between numerical and experimental results, variable face sheet

A less clear result is found when changing the plate material, which is depicted in Fig. 8. For material 2 (EBA) in Fig. 8a the main absorption trends agree, but a substantial difference between experimentally (blue) and numerically (orange) absorption can be found. In the numerical results three local maxima can be found in the absorption spectra. The first and second one are associated with plate resonances and are shifted slightly towards lower frequencies, compared to the experimental results. A possible explanation might be that the material stiffness in the experiment was higher than simulated.

For material 3 (aluminum), depicted in Fig. 8b, two conclusions can be drawn: The numerical setup predicts a Helmholtz resonance near 600 Hz, sharp plate associated absorption peaks near 1450 Hz and 2800 Hz, as well as the higher cavity mode resonance near 3000 Hz. The plate associated absorption peaks are very narrow due to the low material losses inside the aluminum. The Helmholtz resonance associated absorption maxima agree well with the experimentally determined spectrum (blue). In contrast, the plate resonance associated absorption peaks were not found

in the experimental determined absorption. However, additional small absorption peaks are visible around 2000 Hz and 3500 Hz, which might indicate that the plate appeared stiffer in the experiment and was stronger damped due to boundary effects than simulated. In conclusion, we found the numerical model to be able to capture the absorption behavior of the resonator system reasonably well. However, face sheet effects are captured more reliable than plate material effects. This might be owed to varying material parameters such as its thickness or complex stiffness due to manufacturing. Aluminum was not found to be a good alternative to polymers due to its low material damping.

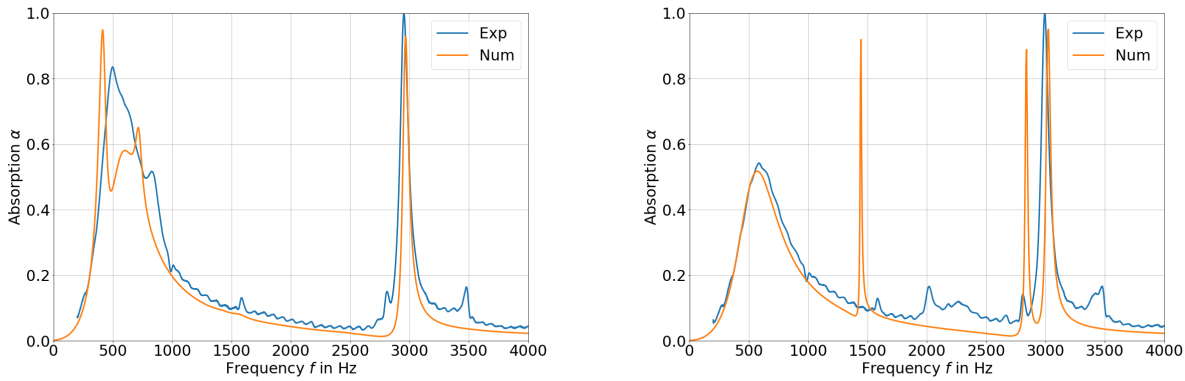

(a) Absorption face sheet I with material 2 (EBA) **(b) Absorption face sheet I with material 3 (Alu)**

Figure 8 Comparison between numerical and experimental results, variable plate material

C. Numerical parameter study

Once validated against the experiments, the numerical model is used to resolve the individual contributions of the main parameters in Table 4 towards the overall absorption. The parameters n, d_{fs} and A_{cav} have not been varied individually as their effect is thought to be captured in the open area ratio σ.

Table 4 Parameter space

face sheet parameters	cavity parameters	plate parameters
$\sigma(d_{\mathrm{fs}}, n, A_{\mathrm{cav}})$	l_{cav_1}	E
d_{fs}	l_{cav_2}	η
h_{fs}	A_{cav}	h_{p}
n		$l_{\mathrm{p}}(A_{\mathrm{cav}})$

1. Influence of face sheet parameters

The influence of different face sheet parameters towards the absorption spectrum of the resonator spectrum is presented in Fig. 9. Changing the face sheet thickness h_{fs} predominantly changes the Helmholtz resonance, as expected from Eq. (1). This is visible in Fig. 9a, where a larger face sheet leads to a lower resonance. While the lower plate resonances near 360 Hz and 470 Hz remain unaffected by a change of the face sheet thickness, one can see that the additional absorption near 1000 Hz is amplified for the thin face sheet when the Helmholtz resonance is nearby. A similar behavior can be identified when looking at a variation of the face sheet open area ratio σ which is shown in Fig. 9b. The plate resonance is largely unaffected by the face sheet porosity, except when the Helmholtz resonance frequency is in the vicinity of a plate resonance. For example, in the case of $\sigma = 2.5\,\%$, the absorption between the lower plate resonances is increased. In the case of $\sigma = 10\,\%$ the Helmholtz resonance frequency is higher and subsequently the higher plate resonance is better excited. These results agree with the experimental results that face sheet parameters

mainly alter the damping near the Helmholtz resonance, which may enable additional plate related damping if the resonances coincide but does not change the plate behavior itself.

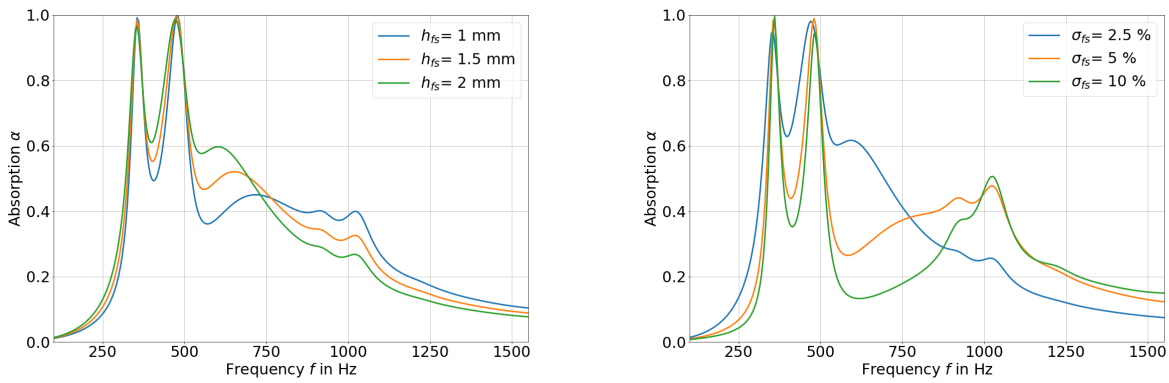

(a) Absorption for variable face sheet thickness h_{fs} **(b) Absorption for variable face sheet open area ratio σ**

Figure 9 Influence of the face sheet parameters

2. Influence of Cavity Depths

Figure 10 displays the influence of the main and second cavity depths onto the overall resonator absorption. In Fig. 10a one can see, that the lower plate resonances are largely unaffected by a decrease of the main cavity depth from 60 mm (green) to 30 mm (blue) and only the Helmholtz resonance is shifted towards higher frequencies. Similar to the face sheet parameters, a higher plate resonance is amplified if the Helmholtz resonance is nearby. On the contrary, when the back cavity depth is increased in Fig. 10b, the Helmholtz resonance frequency is largely unaltered, while the plate resonances are shifted. The two additional low frequency peaks of the system with a back cavity depth of 20 mm (green) are shifted towards higher frequencies if the back cavity depth is decreased to 10 mm (orange). This can be clearly seen at the small local absorption peak near 1100 Hz. The system changes drastically if even smaller back cavities (5 mm, blue) are chosen. In this case only a very minor additional low frequency peak in the absorption spectrum is visible. However, the absorption near the Helmholtz resonance is amplified, as a plate resonance is shifted near the latter. The main effect of the main cavity is therefore a shift of the Helmholtz resonance while a thinner back cavity shifts the plate resonances to higher frequencies. The smaller the back cavity the stronger the effect. Therefore, the main and back cavity depth need to be balanced carefully if the overall cavity depth is constrained. A larger back cavity depth enables stronger narrow very low frequency damping while a larger main cavity allows for lower but broader damping.

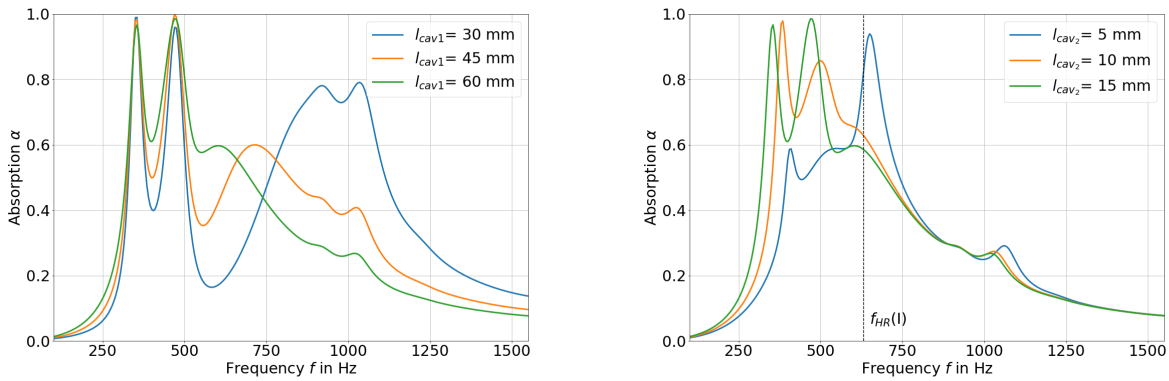

(a) Absorption for variable main cavity depth l_{cav_1}

(b) Absorption for variable back cavity depth l_{cav_2}

Figure 10 Influence of the cavity depths

3. Influence of Flexible Plate

The flexible plate is the central element of the resonator concept. An additional (structural) damping mechanism is introduced, when the flexible plate is made out of a visco-elastic material such as thermoplastics with inherent material losses. The visco-elastic behavior can be described by a complex modulus $E_{\mathrm{C}} = E(1 + \mathrm{i}\eta)$. In Fig. 11 one can see how the complex modulus affects the absorption spectrum.

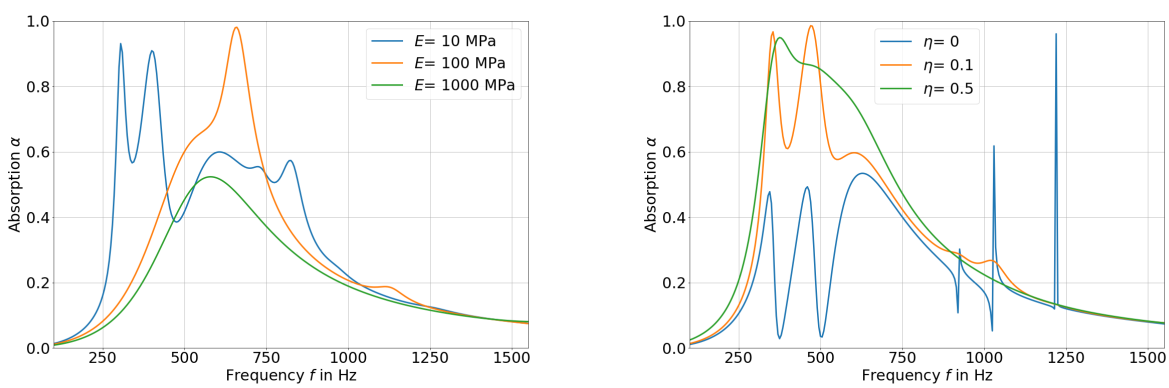

(a) Absorption for variable Young's Modulus E

(b) Absorption for variable material loss factor η

Figure 11 Influence of flexible plate material parameters

Raising the Young's modulus E shifts the overall absorption towards higher frequencies, which is visible in Fig. 11a. In the case of a stiff material with $E = 1000\,\mathrm{MPa}^{\dagger}$, only the Helmholtz resonance is visible. The latter is largely unaffected by a change in the stiffness, although a small shift towards lower frequencies is visible. This is reasonable considering the extremes: A plate with no flexibility in combination with a back cavity can be seen as an enlarged back cavity which leads to a lower Helmholtz resonance. On the other hand, given the flexible plate is very stiff, it acts as a rigid end, the effective overall volume is decreased and the Helmholtz resonance is shifted towards higher frequencies. The choice of the Young's modulus therefore affects the number, frequency and amplitude of additional absorption. For low stiffness values (blue) multiple additional absorption peaks are visible, giving the resonator system more broadband damping. Medium stiffness values (orange) only add one but very strong additional damping peak.

† albeit still flexible compared to e.g. steel with 210 000 MPa

In Fig. 11b a change in the material loss factor η is shown. Interestingly, even without material damping $\eta = 0$, additional damping due to the presence of the flexible plate is introduced into the system. This additional damping is much lower but shows where additional plate resonances occur in the system. However the peaks above 750 Hz are too sharp to be used effectively, as it was shown with the aluminum probe in the experimental results. The low frequency plate damping is drastically increased when material damping $\eta = 0.1$ is introduced. Note, that this is the material damping for the baseline material TPU. In contrast, metals usually have very little inherent losses $\eta \approx 10^{-}3$.

This highlights the need for materials with low stiffness and high material losses for this resonator concept to work effectively against low frequency noise, such as viscoelastic materials or thin metals with additional damping layers.

The impacts of the flexible plate's geometric parameters are depicted in Fig. 12. One can see in Fig. 12a that the

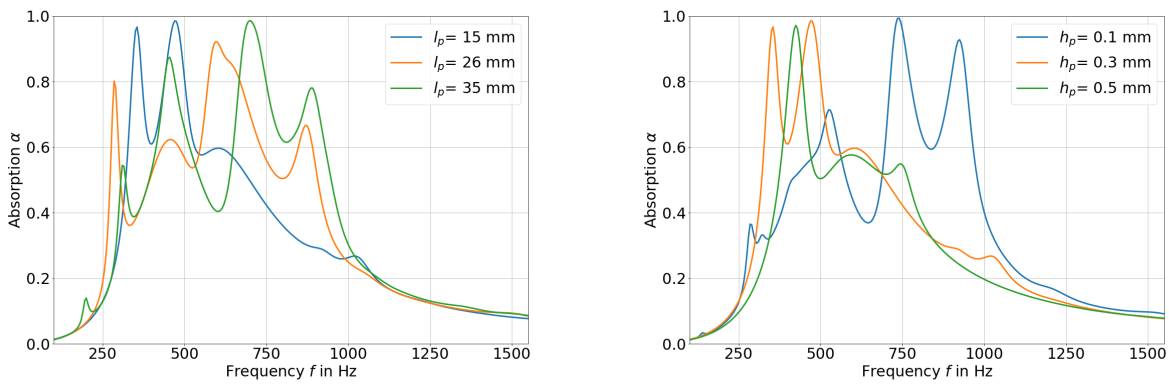

(a) Absorption for variable flexible plate side length **(b) Absorption for variable flexible plate thickness**

Figure 12 Influence of flexible plate geometrical parameters

plate side length has a great impact on the resonance characteristics as it changes the resonance frequencies, as well as the number of relevant absorption maxima. Note that here the smaller side length was varied. Therefore, $l_\mathrm{p} = 26$ mm signifies a square plate. A resonator system with a side length $l_\mathrm{p} = 15$ mm shows two peaks, $l_\mathrm{p} = 22$ mm four and $l_\mathrm{p} = 30$ mm even five peaks, which is in general agreement with Eq. (2). Therefore, the system is very sensitive to the plate size. For broader and more low frequency damping, larger plates are preferred. However, their size has to be matched with the cavity's side or back length.

A similar behavior can be found in Fig. 12b, where thin plates show multi-resonant behavior, as well. However, very thin plates are prone to tear more easily and are hard to install reliably and reproducibly, as stated in [16]. Note that stronger low frequency damping is achieved not with the thinnest plate (blue) but a medium thin (orange) plate. Consequently, the system is also very sensitive to the plate thickness.

V. Conclusion

In this study we investigated the influence of key parameters of a Helmholtz resonator with a flexible wall in a normal incidence tube. The first part of the paper focuses on the experimental investigation of a modular resonator system where the face sheet and the flexible wall material is changed. Additional microphones inside the resonator allowed us to separate between flexible plate and Helmholtz resonance attributed damping. Using this setup, we showed that the flexible plate behaves indifferent from the face sheet for low sound pressure levels which agrees with previous findings from the authors. Additionally, these experimental results were used to validate a numerical model of the system generated with a commercial FEM-Software. This numerical model allowed us to investigate the influence of key parameters of the system with a finer resolution. We found that face sheet parameters such as its thickness or open area ratio in combination with the main cavity mainly influence the Helmholtz resonance. A change in the Helmholtz resonance alters the overall absorption if the corresponding resonance frequency is near dominant plate modes but not their behavior itself. The flexible plate related resonances were found to be very sensitive towards the back cavity as well as plate parameters such as its size and stiffness. On the one hand, this means that special care has to be taken in

the material selection and characterization process. On the other hand, this shows that this liner concept has a very large parameter space to optimize damping for individual purposes. The findings of this study allow for general design rules without resolving the whole parameter space, as well as a deeper understanding of the working principles of this Helmholtz resonator with flexible walls. However, for a realistic liner application the influence of large sound pressure levels and grazing flow need to be taken into account.

Acknowledgements

We want to thank our technician Sebastian Kruck (DLR) for his support regarding the manufacturing of the normal incidence tube and the face sheets. The work presented in this study is part of the PhD project of the first author at TU Berlin and is not related to any contractual work of DLR.

References

[1] Commission, E., for Research, D.-G., and Innovation, *Fly the Green Deal – Europe's vision for sustainable aviation*, Publications Office of the European Union, 2022. https://doi.org/10.2777/732726.

[2] Griffin, S., Lane, S. A., and Huybrechts, S., "Coupled Helmholtz Resonators for Acoustic Attenuation," *Journal of Vibration and Acoustics*, Vol. 123, No. 1, 2001, pp. 11–17. https://doi.org/10.1115/1.1320812.

[3] Zhao, D., "Transmission Loss Analysis of a Parallel-Coupled Helmholtz Resonator Network," *AIAA Journal*, Vol. 50, No. 6, 2012, pp. 1339–1346. https://doi.org/10.2514/1.J051453.

[4] Mi, Y., and Yu, X., "Attenuation of low-frequency sound in U-shaped duct with membrane coupled acoustic resonator: Modeling and analysis," *Journal of Sound and Vibration*, Vol. 489, 2020, p. 115679. https://doi.org/10.1016/j.jsv.2020.115679.

[5] Mizukoshi, F., and Takahashi, H., "Open planar acoustic notch filter using a film-integrated Helmholtz resonator array," *Japanese Journal of Applied Physics*, Vol. 62, No. 3, 2023, p. 034002. https://doi.org/10.35848/1347-4065/acc0b7.

[6] Palani, S., Subramanyam, R. R., Paruchuri, C., and Joseph, P., "Flexible Membrane Type Non-Linear Liner," *29th International Congress of Sound and Vibration*, 2023.

[7] Solano, C., and Cattafesta, L., "Modeling, design, and optimization of a dielectric elastomer acoustic liner," *International Journal of Aeroacoustics*, Vol. 22, No. 5-6, 2023, pp. 599–620. https://doi.org/10.1177/1475472X231199187.

[8] Horowitz, S. B., Nishida, T., Cattafesta, L. N., and Sheplak, M., "Characterization of a Compliant-Backplate Helmholtz Resonator for an Electromechanical Acoustic Liner," *International Journal of Aeroacoustics*, Vol. 1, No. 2, 2002, pp. 183–205. https://doi.org/10.1260/147547202760236969.

[9] Liu, F., Horowitz, S., Nishida, T., Cattafesta, L., and Sheplak, M., "A multiple degree of freedom electromechanical Helmholtz resonator," *The Journal of the Acoustical Society of America*, Vol. 122, No. 1, 2007, pp. 291–301. https://doi.org/10.1121/1.2735116.

[10] Nudehi, S. S., Duncan, G. S., and Farooq, U., "Modeling and Experimental Investigation of a Helmholtz Resonator with a Flexible Plate," *Journal of Vibration and Acoustics*, Vol. 135, No. 4, 2013. https://doi.org/10.1115/1.4023810.

[11] Sanada, A., and Tanaka, N., "Extension of the frequency range of resonant sound absorbers using two-degree-of-freedom Helmholtz-based resonators with a flexible panel," *Applied Acoustics*, Vol. 74, No. 4, 2013, pp. 509–516. https://doi.org/10.1016/j.apacoust.2012.09.012.

[12] Kohlenberg, F., Schulz, A., Enghardt, L., and Knobloch, K., "Modeling of Advanced Helmholtz Resonator Liners with a Flexible Wall," *AIAA Journal*, Vol. 61, No. 7, 2023, pp. 3108–3118. https://doi.org/10.2514/1.J062227.

[13] Hossain, M. R., Ross, E. P., and Bennett, G. J., "Acoustic plate-valve resonator for low-frequency sound absorption," *AIP Advances*, Vol. 13, No. 6, 2023. https://doi.org/10.1063/5.0142908.

[14] Knobloch, K., Enghardt, L., and Bake, F., "Investigation of Flexible Walls for Acoustic Liners," *AIAA-2019-2565*, 25th AIAA/CEAS Aeroacoustics Conference, June 2019. https://doi.org/10.2514/6.2019-2565.

[15] Kohlenberg, F., Radmann, V., Genßler, J., Enghardt, L., and Knobloch, K., "Experimental and Numerical Analysis of the Vibro-Acoustic Behavior of a Helmholtz Resonator with a Flexible Wall," *AIAA AVIATION 2023 Forum*, American Institute of Aeronautics and Astronautics, Reston, Virginia, 2023. https://doi.org/10.2514/6.2023-3348.

[16] Genßler, J., Kohlenberg, F., Knobloch, K., and Enghardt, L., "Experimental Investigations of Flexible Wall Effects in Helmholtz Resonators for Aircraft Engine Acoustic Liners," *AIAA AVIATION 2023 Forum*, American Institute of Aeronautics and Astronautics, Reston, Virginia, 2023. https://doi.org/10.2514/6.2023-3347.

[17] Ingard, U., "On the Theory and Design of Acoustic Resonators," *The Journal of the Acoustical Society of America*, Vol. 25, No. 6, 1953, pp. 1037–1061. https://doi.org/10.1121/1.1907235.

[18] Blevins, R. D., *Formulas for dynamics, acoustics and vibration*, Wiley series in acoustics noise and vibration, Wiley, Chichester (UK), 2016. https://doi.org/10.1002/9781119038122.

[19] Dokumaci, E., "A note on transmission of sound in a wide pipe with mean flow and viscothermal attenuation," *Journal of Sound and Vibration*, Vol. 208, No. 4, 1997, pp. 653–655. https://doi.org/10.1006/jsvi.1997.1043.

[20] Comsol Multiphysics 6.1, "Acoustics Module User's Guide," , 2022.

[21] Crandall, I. B., *Theory of Vibrating Systems and Sound*, D. Van Nostrand Company, 1926.

[22] Fock, V. A., "A Theoretical Investigation of the Acoustical Conductivity of a Circular Aperture in a Wall put across a Tube," *Comptes Rendus (Doklady) de l'Académie des Sciences de l'URSS*, Vol. Volume XXXI, No 9, 1941, pp. 875–878.

[23] Kohlenberg, F., Schulz, A., Enghardt, L., and Knobloch, K., "Modelling of Acoustic Liners Consisting of Helmholtz Resonators Coupled with a Second Cavity by Flexible Walls," *28th AIAA/CEAS Aeroacoustics 2022 Conference*, American Institute of Aeronautics and Astronautics, Reston, Virginia, 2022. https://doi.org/10.2514/6.2022-2824.